Ion Dynamics Underlying the Seizure Delay Effect of Low-Frequency Electrical Stimulation

Guillaume Girier[1,✉], **Isa Dallmer-Zerbe**[1, 2,], **Jan Chvojka**[2,], **Jan Kudláček**[2,], **Přemysl Jiruška**[2,], **Jaroslav Hlinka**[1,3], **and Helmut Schmidt**[1,]

[1]Department of Complex Systems, Institute of Computer Science of the Czech Academy of Sciences, Prague, Czech Republic
[2]Department of Physiology, Second Faculty of Medicine, Charles University, Prague, Czech Republic
[3]National Institute of Mental Health, Klecany, Czech Republic

The biological mechanisms underlying the spontaneous and recurrent transition to seizures in the epileptic brain are still poorly understood. As a result, seizures remain uncontrolled in a substantial proportion of patients. Brain stimulation is an emerging and promising method to treat various brain disorders, including drug-refractory epilepsy. Selected stimulation protocols previously demonstrated therapeutic efficacy in reducing the seizure rate. The stimulation efficacy critically depends on chosen stimulation parameters, such as the time point, amplitude, and frequency of stimulation. This study aims to explore the neurobiological impact of 1Hz stimulation and provide the mechanistic explanation behind its seizure-delaying and seizure-suppressing effects. We study this effect using a computational model, a modified version of the Epileptor-2 model, in close comparison with such stimulation effects on spontaneous seizures recorded *in vitro* in a high-potassium model of ictogenesis in rat hippocampal slices. In particular, we investigate the mechanisms and dynamics of spontaneous seizure emergence, the seizure-delaying effect of the stimulation, and the optimal stimulation parameters to achieve the maximal anti-seizure effect. We show that the modified Epileptor-2 model replicates key experimental observations, and captures seizure dynamics and the anti-seizure effects of low-frequency electrical stimulation (LFES) observed in hippocampal slices. We identify the critical thresholds in the model for seizure onset and determine the optimal stimulation parameters – timing, amplitude, and duration – that exceed specific thresholds to delay seizures without triggering premature seizures. Our study highlights the central role of sodium-potassium pump dynamics in terminating seizures and mediating the LFES effect.

epilepsy | low-frequency electrical stimulation | seizure suppression | bifurcation analysis | mathematical model

Correspondence: ***girier@cs.cas.cz***

Introduction

Epilepsy is a common neurological disorder with an incidence rate of 61.4 per 100,000 person-years (1, 2). Around 30% of epilepsy patients do not respond to anti-seizure medications (3). Furthermore, only 4.5% of patients are eligible for brain surgery, which is a second-line treatment of epilepsy and a highly invasive procedure (4). Thus, there is a need for the development of new and safe treatment options for epilepsy (5).

Brain stimulation has proven its effectiveness in reducing the seizure rate (6, 7). However, this effectiveness is highly patient- and stimulation parameter-specific, calling for a personalized approach to brain stimulation and epilepsy treatment in general (5, 7). Moreover, the exact cellular and network effect of brain stimulation remains insufficiently understood. This precludes a rational design of stimulation protocols, which is currently replaced by trial-and-error procedures in both the development of new stimulation protocols, as well as in clinical practice (7, 8). To overcome these current challenges in epilepsy treatment, computational modeling has proven advantageous for gaining mechanistic insight and allowing for a safe, inexpensive, and extensive exploration of treatment parameters in the virtual environment (8–10).

In the context of brain stimulation treatment for epilepsy, Low-Frequency Electrical Stimulation (LFES) has been reported to have an inhibitory effect on epileptic activity in models of acute seizures, chronic epilepsy models (11, 12), and in patients with medically intractable seizures (13–16). It thus could serve as a candidate for a new treatment option in epilepsy. However, it appeared that LFES could also trigger epileptic activity (7, 14, 17, 18). Previous studies have shown how this dual effect of stimulation in epileptic tissue is critically dependent on the timing, duration, and amplitude of stimulation, e.g., such that stimulation early after seizure offset would have a seizure-delaying effect while acting in a seizure-promoting fashion when delivered close to an expected seizure onset (9, 19, 20).

The goal of the current study is to investigate and explain the effects of LFES and predict its optimal parameters to delay seizures in local-field potential recordings (LFP) of hippocampal rat brain slices under high-potassium condition, a commonly used animal model of

focal epilepsy. To understand the spontaneous seizure dynamics arising from the high-potassium conditions, a biophysical model was employed that is capable of tracking the potassium dynamics, as well as other ion dynamics, linked to the neuronal population activity of excitatory and inhibitory cell populations as recorded by the LFP signal. Various works (20–24) have studied the effect of LFES in mathematical models of epilepsy, and in particular in the Epileptor-2 model (12, 25).

First, we focus on the emergence of spontaneous seizure-like events recorded in hippocampal slices, and the repeated transitions between the interictal and ictal state. Concurrently, the model parameters are optimized to reproduce the different characteristics of the individual slices, explaining their heterogeneity. Second, we demonstrate that the model can accurately capture the seizure-delaying effect of LFES. By stabilizing the system into a seizure-free attractor, LFES is shown to stop extracellular potassium accumulation by balancing the effect of sodium-potassium pumps, thereby preventing seizure generation.

Materials and Methods

Experimental Design. Brain slices were obtained from four male Wistar rats weighing approximately 200g. The animals were kept in an enriched environment with 12/12 hours of light and darkness and regularly checked for health status prior to the experiment. The animals were anesthetized (80 mg/kg ketamine, 25 mg/kg xylazine) and decapitated. The brains were extracted from the skull and placed into an ice-cold, oxygenated protective solution – sucrose-based artificial cerebrospinal fluid – which contained (in mM) 189 mM sucrose, 10 glucose, 2.5 KCl, 0.1 $CaCl_2$, 5 $MgCl_2$, 26 $NaHCO_3$, and 1.25 NaH_2PO_4*H_20. The brain was then cut into saggital slices of 350 μm thickness using a vibratome (Campden Instruments, Loughborough, UK). The CA3 region was then cut off by a scalpel since the data was recorded for another study (19). Then, the hippocampal slices were moved to a holding chamber at room temperature filled with normal artificial cerebrospinal fluid (ACSF) and continuously aerated with a humidified mixture of 95% O_2 and 5% CO_2. The ACSF contained (in mM) 125 NaCl, 26 $NaHCO_3$, 3 KCl, 2 $CaCl_2$, 1 $MgCl_2$, 1.25 NaH_2PO_4, and 10 glucose. After at least 60 minutes, a slice was transferred to a recording interface chamber at 34 ± 1°C containing normal ACSF. They were left at rest for 10 minutes before experiments started. Local field potentials were recorded using a glass micropipette (diameter 10 - 15 μm) filled with ACSF and inserted in the stratum pyramidale of the CA1 subregion. The signal was amplified using Model 3000 AC/DC Differential Amplifier (A-M Systems, Inc., Carlsborg, Washington, USA), digitized at 10 kHz sampling frequency using Power1401 (CED, Cambridge, UK) and recorded using Spike2 software (CED, Cambridge, UK). To induce epileptic activity, we added KCl solution at first in large steps (1 - 3 mM) until a total concentration of 6.5 - 7 mM was reached. After that, we gradually increased the concentration (0.2–0.5 mM at a time) until spontaneous seizure-like episodes appeared. The experimental protocol included perturbations of the CA1 network with regularly delivered stimuli to Schaffer collaterals (input to CA1) with a frequency of 1 Hz. The stimuli were electrical pulses of 200 μs duration using a bipolar silver wire electrode and isolated constant current stimulator (Digitimer Ltd., Welwyn, UK). The stimulation was initiated immediately after the end of a seizure-like event, at the beginning of the inter-seizure interval (ISI). A stimulated ISI was typically followed by an ISI without stimulation and vice versa. In the analysis, each stimulated ISI was matched to the preceding control ISI. The stimulation duration ranged from a few seconds to nearly two minutes. Table 1 summarizes basic data characteristics. The signals were subsequently analyzed using custom-written Matlab scripts.

All experimental procedures were approved by the Czech Academy of Sciences Ethics Committee and the Ethics Committees of the Second Faculty of Medicine (Project Licence No. MSMT-31765/2019-4).

Statistical Analysis. To test whether there is a seizure-delaying effect due to LFES in the experimental data, we computed the Spearman correlation between stimulated ISIs and ISI prolongation for each slice separately. The latter was calculated as percent change of the stimulated ISI with respect to the control ISI. We report the correlation coefficient r and the associated p-values. The model analysis did not require any statistical analysis.

Model Design. In this study, we aimed to investigate a minimal biophysical model of a neuronal population that: 1) exhibits epileptiform activity similar to our data, 2) is based on the potassium concentration dynamics, and 3) can produce a seizure delay by low-frequency electrical stimulation.

We chose a modified version of the Epileptor-2

	K_{bath}	n_{seiz} pre-stim	n_{seiz} stim	ISI pre-stim	ISI control	ISI stim	stim length
Slice 1	9.5 mM/L	5	28	64 ± 3 s	56 ± 5 s	78 ± 26 s	51 ± 24 s
Slice 2	8.6 mM/L	8	15	58 ± 12 s	46 ± 7 s	73 ± 23 s	40 ± 22 s
Slice 3	8 mM/L	10	21	56 ± 2 s	53 ± 6 s	75 ± 22 s	58 ± 25 s
Slice 4	5.3 mM/L	6	22	43 ± 9 s	34 ± 6 s	45 ± 10 s	27 ± 12 s

Table 1. Data characteristics per slice. ISI and stimulation (stim) length values per slice (mean ± standard deviation; ISI pre-stim: ISI before stimulation protocol, ISI stim: ISI with stimulation, ISI control: ISI without stimulation preceding an ISI with stimulation, used as reference for relative ISI changes). K_{bath} marks the final potassium concentration per slice, which was sufficient to elicit seizure-like events.

model (25):

$$\begin{aligned}
\tau_m \frac{\mathrm{d}V}{\mathrm{d}t} &= u(V, x_\mathrm{D}, [K^+]_\mathrm{o}) - g_\mathrm{L} V + g_\mathrm{stim} I_\mathrm{stim}(t), \\
\frac{\mathrm{d}x_\mathrm{D}}{\mathrm{d}t} &= \frac{(1-x_\mathrm{D})}{\tau_x} - \delta_x x_\mathrm{D} \upsilon_i(V), \\
\frac{\mathrm{d}[K^+]_\mathrm{o}}{\mathrm{d}t} &= \frac{K_\mathrm{bath} - [K^+]_\mathrm{o}}{\tau_K} \\
&\quad - 2\gamma I_\mathrm{pump}([K^+]_\mathrm{o}, [Na]_\mathrm{i}) + \delta_K \upsilon_i(V), \\
\frac{\mathrm{d}[Na^+]_\mathrm{i}}{\mathrm{d}t} &= \frac{[Na^+]_\mathrm{i}^0 - [Na^+]_\mathrm{i}}{\tau_{Na}} \\
&\quad - 3 I_\mathrm{pump}([K^+]_\mathrm{o}, [Na^+]_\mathrm{i}) + \delta_{Na} \upsilon_i(V),
\end{aligned} \tag{1}$$

where V is the average membrane potential of pyramidal cells, x_D is the synaptic resource, and $[K^+]_\mathrm{o}$ and $[Na^+]_\mathrm{i}$ are the extracellular potassium and intracellular sodium concentrations, respectively.

The membrane potential V is driven by the potassium concentration $[K^+]_\mathrm{o}$ and synaptic input, which is concisely expressed by

$$\begin{aligned}
u(V, x_\mathrm{D}, [K^+]_\mathrm{o}) = g_K 26.6\mathrm{mV} \log\left(\frac{[K^+]_\mathrm{o}}{[K^+]_\mathrm{o}^0}\right) \\
+ I_{exc}(V, x_\mathrm{D}) + I_{inh}(V),
\end{aligned} \tag{2}$$

where the first term is the potassium depolarizing current, and I_{exc} and I_{inh} are the excitatory and inhibitory synaptic inputs to the excitatory population. The excitatory synaptic input I_{exc} is defined as:

$$I_{exc}(V, x_\mathrm{D}) = g_{exc} \upsilon_i(V) x_\mathrm{D}, \tag{3}$$

with g_{exc} being the conductance of excitatory synapses, and $\upsilon_i(V)$ being the firing rate of the excitatory population. We note here that the excitatory synaptic input is current-based, since the reversal potential for excitatory synapses is so large that its difference from the membrane potential can be considered roughly constant (26).

The inhibitory synaptic input I_{inh} is defined as (27):

$$I_{inh}(V) = g_{inh}(V_{inh} - V), \tag{4}$$

with g_{inh} being the conductance of inhibitory synapses, and V_{inh} their reversal potential.

The firing rate function $\upsilon_i(V)$ is chosen to be a sigmoid function with threshold V_{th} and maximum firing rate υ_{max}:

$$\upsilon_i(V) = \frac{\upsilon_{max}}{1 + ^{V_{th} - V}}. \tag{5}$$

The excitatory population is also subjected to low-frequency stimulation, $I_{stim}(t)$. Each stimulus is represented by a Dirac delta function, and the sequence of stimuli thus reads $I_{stim}(t) = A \sum_n \delta(t - t_n)$, where t_n represents stimulation times (every 1s in our protocol), and A is the stimulation amplitude. The parameter g_{stim} was added to ensure dimensional consistency within the model, thereby preserving the physical coherence of the equations and their underlying biophysical interpretation.

Lastly, the activity of the Na-K pump is computed as follows (28):

$$\begin{aligned}
I_{pump}([K^+]_\mathrm{o}, [Na^+]_\mathrm{i}) = \\
\frac{\rho}{(1 + ^{3.5 - [K^+]_\mathrm{o}})(1 + ^{(25.0 - [Na^+]_\mathrm{i})/3})}.
\end{aligned} \tag{6}$$

We made two modifications to the original Epileptor-2 model (25). First, we changed the firing rate function to a simple sigmoid function, which allows for non-zero firing rates even at small values of the membrane potential. The second modification concerns the implementation of inhibition. The original Epileptor-2 model features a non-depressing inhibitory neuronal population whose activity is proportional to that of the excitatory neuronal population, thus providing a tight balance between the inhibitory and excitatory population. Here, however, we chose an inhibitory population that exhibits a constant firing rate and acts on the excitatory population via

conductance-based synapses. Since the reversal potential V_{inh} is close to the resting potential at low $[K^+]_o$ concentrations, inhibition doesn't produce strong hyperpolarizing synaptic potentials. Rather, it has a shunting effect that is roughly proportional to the depolarization of the membrane. Experimental and computational evidence suggests that shunting inhibition is prevalent in the hippocampus, and that it plays a crucial role in the robustness of γ-oscillations (29, 30).

One of the objectives is to investigate the effect of potassium on the neuronal population. In the full model, the sodium and potassium concentrations are slowly changing variables that can be assumed to be roughly constant on the much faster time scales that govern the dynamics of V and x_{D}. Therefore, to describe the characteristic dynamics of V and x_{D}, we will assume that $[K^+]_o$ and $[Na^+]_i$ are time-invariant, leading to the following set of equations:

$$\begin{aligned}
\tau_m \frac{\mathrm{d}V}{\mathrm{d}t} &= u(V, x_{\mathrm{D}}, [K^+]_{\mathrm{o}}) - g_{\mathrm{L}} V + g_{\mathrm{stim}} I_{\mathrm{stim}}, \\
\frac{\mathrm{d}x_{\mathrm{D}}}{\mathrm{d}t} &= \frac{(1 - x_{\mathrm{D}})}{\tau_x} - \delta_x x_{\mathrm{D}} \upsilon_i(V), \\
\frac{\mathrm{d}[K^+]_{\mathrm{o}}}{\mathrm{d}t} &= 0, \\
\frac{\mathrm{d}[Na^+]_{\mathrm{i}}}{\mathrm{d}t} &= 0,
\end{aligned} \tag{7}$$

This system allows us to obtain the bifurcation structure of the system with respect to the ion concentration which can be studied as parameters.

In this analysis, we consider two scenarios: 1) using parameter sets fitted to the experimental data (for Slices 1 to 4) and 2) using an arbitrary parameter set to explore LFES in greater detail, referred to as Slice M0. The parameters that are kept constant throughout the analysis are shown in Table 2.

The parameters specific to the Slice M0 and the ones specific to the experimental Slices 1-4 are shown in Table 3.

Code and Data Accessibility. All code supporting the findings of this study are publicly available at https://github.com/GuillaumeGirier/Low-Frequency-Electrical-Stimulation-and-Seizure-Delay repository. The experimental data will be made available at the time of publication.

Results

The emergence of spontaneous seizure transitions. In the first analysis, we examine the spontaneous transitions into seizures by analyzing how the model parameters influence the duration of seizures and ISIs. To achieve this, we will first establish precise definitions for what constitutes a seizure and an ISI, both in the data and within the framework of the model.

The ISI was defined as the time interval in seconds between the end of one seizure and the beginning of the next. In the data, seizure offsets were automatically identified by finding the minimum in the LFP (using Matlab R2021a's *islocalmin()* function with 'MinProminence' set to half the signal span and a 'MinSeparation' 20 seconds, applied to the smoothed signal; *smooth()* with window size of one second). Seizure onsets were identified by finding the steep increase of LFP (using *findchangepts()* function with 'Statistic' set to 'linear') in the time window of up to 30 seconds before each identified seizure offset. Examples of identified seizure on- and offsets can be seen in the Fig. 3.A. We use equivalent criteria in the model time series: the minimum is determined from the first derivative of the time series, and the seizure onset is identified as the crossing of the membrane potential through V_{th} (see Fig. 3.C).

Fig. 1.A shows four example LFP recordings, obtained from the experimental setup described in Section . It shows the heterogeneity in terms of ISI and seizure duration between slices, which is dependent on the amount of added potassium. Based on this observation, we decided to match the recordings with the model in terms of seizure duration and ISI.

The Epileptor-2 model contains various parameters that can be modified to change the temporal structure of the epileptic activity and thus replicate the experimental observations. In our case, we focus on the firing threshold V_{th} and the maximum firing rate υ_{max}. It is reasonable to assume that slices differ in specific characteristics (31–34), such as cellular excitability and network connectivity, due to intrinsic biological heterogeneity and variations in preparation protocols. This variability underscores the importance of systematically analyzing the parameters V_{th} and υ_{max} to account for the diversity observed in the dataset.

The heatmaps in Fig. 1.B determine the slice-specific length of the ISI and seizures as V_{th} and υ_{max} are varied, demonstrated for slices 1 and 4 with their respective values of K_{bath}. We note here that if the ISI and seizure length are equal to zero, the model exhibits con-

Parameter	Description	Value
γ	Extracellular/intracellular potassium volume ratio	10
δ_K	Concentration increments at spike for potassium dynamics	0.02 mM
δ_{Na}	Concentration increments at spike for sodium dynamics	0.03 mM
δ_x	Resource increments at spike for synaptic depression	0.01
K_{bath}	Potassium concentration in the bath	8.5 mM
$[K^+]_o^0$	Resting extracellular potassium concentration	3.0 mM
$[Na^+]_i^0$	Resting intracellular sodium concentration	10.0 mM
τ_K	Time constant for potassium dynamics	17.5 s
τ_{Na}	Time constant for sodium dynamics	35.0 s
τ_m	Time constant for membrane potential	0.002 s
τ_x	Time constant for synaptic depression	2.0 s
ρ	Maximum pump flux	0.1142 mM/s
υ_{max}	Maximal rate of the firing rate function	75.0 Hz
V_{th}	Threshold potential	10.0 mV
g_L	Conductance of the leak flux	1.0
g_K	Conductance of the potassium flux	0.5
g_{exc}	Conductance of the excitatory population	0.3
g_{inh}	Conductance of the inhibitory population	0.1686
g_{stim}	Conductance of the stimulation	1Ω
V_{inh}	Reversal potential of the inhibitory population	-15 mV

Table 2. Fixed parameter set used in Result Section.

stant activity with either a low or high firing rate. For any fixed value of υ_{max}, while we decrease V_{th} in such a way that the system passes through the epileptic domain, the length of the ISI decreases and the seizure length increases, until it finally reaches a continuous high firing state.

Using the heatmaps presented in Fig. 1.B, we calibrate the model to match two examples from Fig. 1.A (slice 1 and 4). In Fig. 1.C and D, we first show a time series of the LFP from the data, then a time series of the membrane potential from the model. One can notice the similarity in structure of the epileptic activity of the model: a slow depolarization that characterizes the ISI, then a fast depolarization that starts the seizure. The seizure itself is characterized by initially further depolarization, and subsequent repolarization until the membrane potential reaches its minimum, which terminates the seizure. It exhibits very similar sodium and potassium concentrations as determined experimentally (35). We note here that the resting sodium concentration in the model is 10mM, which is representative of the normal physiological state. In addition to characterizing the dynamics of potassium and sodium ions, the model provides access to the firing rate and the activity of the Na-K pumps. Shortly before a seizure, the firing rate shows a modest increase, followed by a rapid upturn at the beginning of the seizure. At the end of the seizure, the firing rate declines abruptly. In parallel, Na-K pump activity gradually increases during the seizure. At the seizure end, pump activity initially decreases rapidly as the membrane potential returns to baseline. After reaching baseline, the activity continues to decline but at a slower steady rate.

The comparison of the subpanels in Fig. 1.B highlights the modeled effect of increasing extracellular potassium in the bath containing the slices. If we define fixed parameters for V_{th} and υ_{max} to fit a single slice, the model predicts that at low potassium concentrations, seizures do not occur. However, as potassium levels are increased, the epileptic domain expands progressively until the model begins to exhibit seizure activity. We can, therefore, assume that potassium modifies the excitability of a population of neurons *in vitro* in such a way that the epileptic domain is extended. These results demonstrate the importance of potassium addition in the emergence of the epileptic process, and therefore, in the subsequent analysis, we focus on replicating experimental data derived from sequential increases in extracellular potassium levels, using slow potassium ramp simulations to uncover pivotal thresholds governing seizure onset.

In Fig. 2.A, we first test different values of K_{bath} to study their effect on the time series. The potassium concentration in the surrounding bath, K_{bath}, is in-

Parameter	Description	M0	1	2	3	4
K_{bath}	Potassium concentration in the bath	8.5 mM	9.5mM	8.6mM	8mM	5.3mM
V_{th}	Threshold potential	10mV	14mV	12mV	10mV	2.4mV
υ_{max}	Maximal rate of the firing rate function	75Hz	80Hz	70Hz	70Hz	35Hz
g_{inh}	Conductance of the inhibitory population	0.1686	0.05	0.05	0.05	0.1686

Table 3. Specific parameter set used to fit the experimental data.

creased instantaneously at the vertical dashed line. Similar to what we described for the previous figure, we note that the addition of potassium allows the appearance of seizures only when a specific concentration threshold is exceeded, then the ISI progressively reduces and the seizure increases in length until the added potassium stabilizes the potential at a high frequency value. This status could correspond to so-called *status epilepticus*, i.e. an epileptic seizure prolonged for more than 5 minutes or by repeated seizures without regaining consciousness between them (36–38). We remark here that the alternative scenario of depolarisation block is not captured by our model, because the firing rate saturates at high values of the membrane potential, which represents intense firing activity. Note that the length of ISI and seizure duration depend also on the V_{th} and υ_{max}, which is fitted individually to each slice in Fig. 1.C,D. For each setting of V_{th} and υ_{max} the effect of increasing K_{bath} corresponds to the one shown in Fig. 2.A. Comparing K_{bath} concentrations between slices, we found longer ISI and shorter seizures for higher K_{bath}, while increasing K_{bath} within one slice will lead to shorter ISI and longer seizure length. This discrepancy is resolved when considering that each slice has different characteristics, which corresponds to different parameter combinations placing it in a different point in Fig. 1.B.

In the next step, we focus on the potassium addition protocol: in Fig. 2.B, the experimental protocol (blue curve), which corresponds to regular additions in the medium with a delay long enough to allow the potassium to diffuse into the tissue, is superimposed onto our protocol applied to the model (black curve). In the experimental protocol, potassium is added until the first appearance of spontaneous, recurring seizures. However, sometimes the experimenter probed the tissue excitability by stimulating the tissue in order to induce the appearance of seizures, as commonly done in epilepsy research and clinical practice (39). In order to reproduce the experimental setup, we added a constant slow input of potassium to our model respecting the same values of time and potassium necessary to have seizures. The slow addition of potassium in the model, as opposed to the step-wise manner during the experiment, is justified by the slow diffusion process at each step, so we can assume that our process is similar. Furthermore, we tested the induction of seizures by external stimulation with single spikes of 30mA, which are indicated in Fig. 2.B by red dashed vertical lines.

We first examine the effect of the experimental protocol. Fig. 2.C shows the recorded LFP from Slice 3, overlaid with the different stimulations applied to induce seizures. Single-pulse stimulations, depending on the timing, were insufficient to trigger seizure activity. At low potassium concentrations, such stimulations produced only transient depolarization-repolarization responses. However, repeated stimulations were capable of provoking seizure events under these conditions.

In Fig. 2.D, the experimental protocol is reproduced in the model, showing the membrane potential of the population. When stimulating with single pulses, we notice that if the potassium value is too low, then only stimulation artifacts are observable. However, if these single pulses occur at higher potassium concentrations, seizures are induced.

The anti-seizure effect of LFES. To demonstrate the seizure-delaying effect of LFES, we analyzed the LFP recordings with regards to a difference in length between stimulated ISIs and control ISIs (which are ISIs without stimulation preceding the stimulated ISI). ISI prolongation was calculated as percent change of the stimulated ISI with respect to the control ISI.

We find that stimulated ISIs were significantly longer than the control ISIs, in each of the slices, as assessed via Spearman correlation (see Fig. 3.B and Table 2; see also Supplemental Material S1). This indicates that the 1 Hz stimulation indeed had a seizure delaying, or anti-seizure, effect. Fig. 3.A shows two examples of control and subsequent stimulated ISI (their beginnings and ends marked by red and green vertical lines, respectively). The longer stimulation in example 2 leads to a substantially longer stimulated ISI as compared to control ISI.

In Fig. 3.C and D, we apply the LFES protocol to the model. In all the simulations, the stimulation is applied right after the seizure. In Fig. 3.C, we can observe that

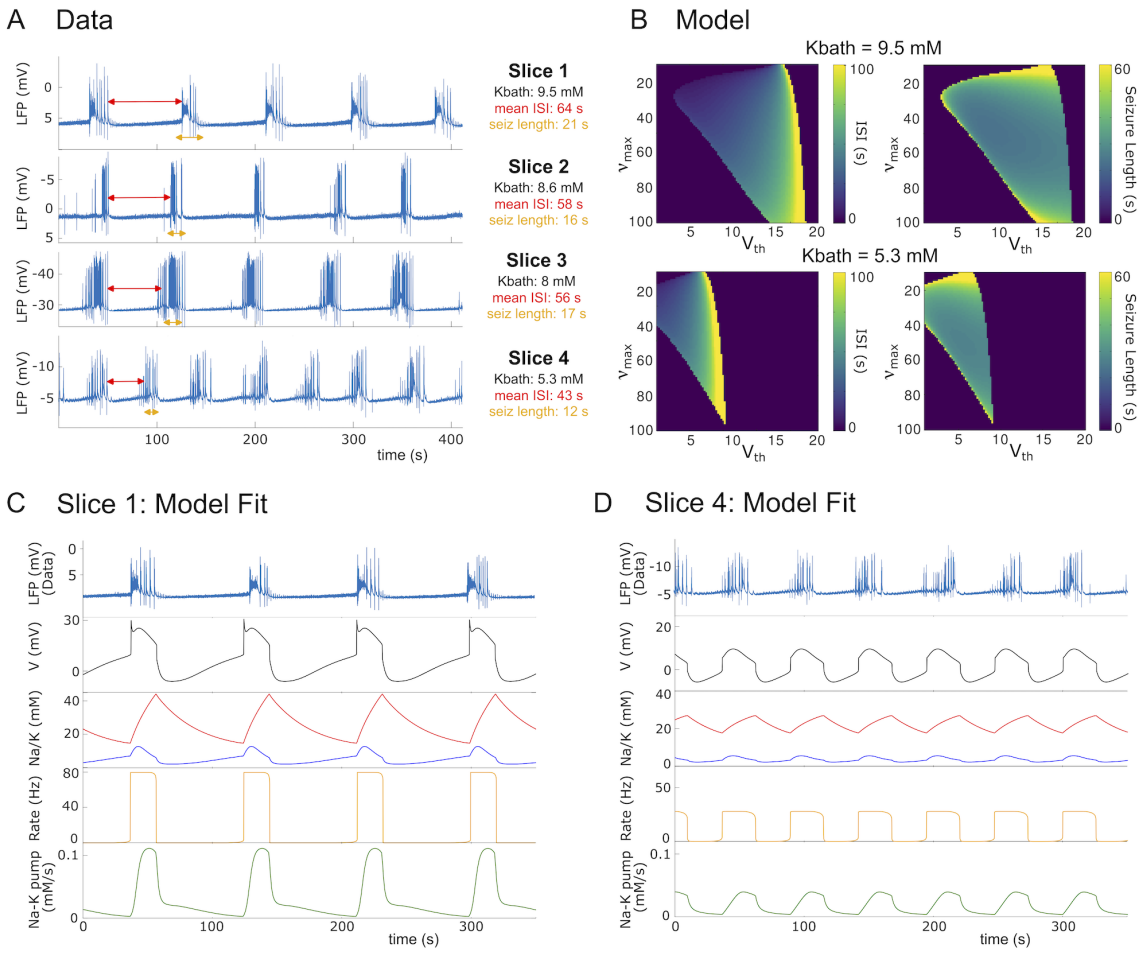

Fig. 1. Fitting model ISI and seizure duration to the data. (A) Time series of data from different slices. Red double arrows indicate ISIs, and orange double arrows indicate seizures. (B) Heatmaps of ISI and seizure duration with respect to the parameters v_{max} and V_{th}, for $K_{bath} = 9.5$ and $K_{bath} = 5.3$. (C) Model fit to Slice 1. (D) Model fit to Slice 4. In these panels, red curves refer to $[Na^+]_i$ concentration, and the blue curves refer to $[K^+]_o$ concentration. For the specific parameters for each slice, see Table 3.

the stimulation pulse does not have an immediate effect for approximately the first 10 to 15s. Only after this initial period, we observe a tangible effect of the stimulation, which is an increase in the depolarization rate. Then, we observe a depolarization, a small hyperpolarization and then the convergence of the system onto a new forced equilibrium until the stimulation ends. Thus there exists an optimal time window in which the stimulation is effective, which we investigate further below and in Fig. 5.C.

Fig. 3.D shows the effect of stimulation on the ISI in the same way as panel B. For values up to $t_{stim} = 10$s, the stimulation does not have an effect on the ISI, in line with the (descriptive) experimental observations in Fig. 3.B that for short stimulation lengths LFES is ineffective. For stimulation periods greater than $t_{stim} = 10$s, in the case of Slices 1 to 3, the ISI increases linearly with the stimulation period. The model reproduces the same order of slope as observed in the experimental data (Data: $\text{Slope}_{\text{Slice1}}$ =0.830, $\text{Slope}_{\text{Slice2}}$ =0.933, $\text{Slope}_{\text{Slice3}}$ =0.937; Model: $\text{Slope}_{\text{Slice1}}$ =1.027, $\text{Slope}_{\text{Slice2}}$ =1.183, $\text{Slope}_{\text{Slice3}}$ =1.268). This demonstrates its ability to predict the individual effectiveness of the anti-seizure protocol. However, in the case of Slice 4, the ISI decreases and then stabilizes, as LFES induces an early seizure. This phenomenon arises from the choice of parameters optimized to fit the experimental data. The impact of LFES on seizure delay as a function of V_{th} and v_{max} will be examined in the Supplemental Material S2.

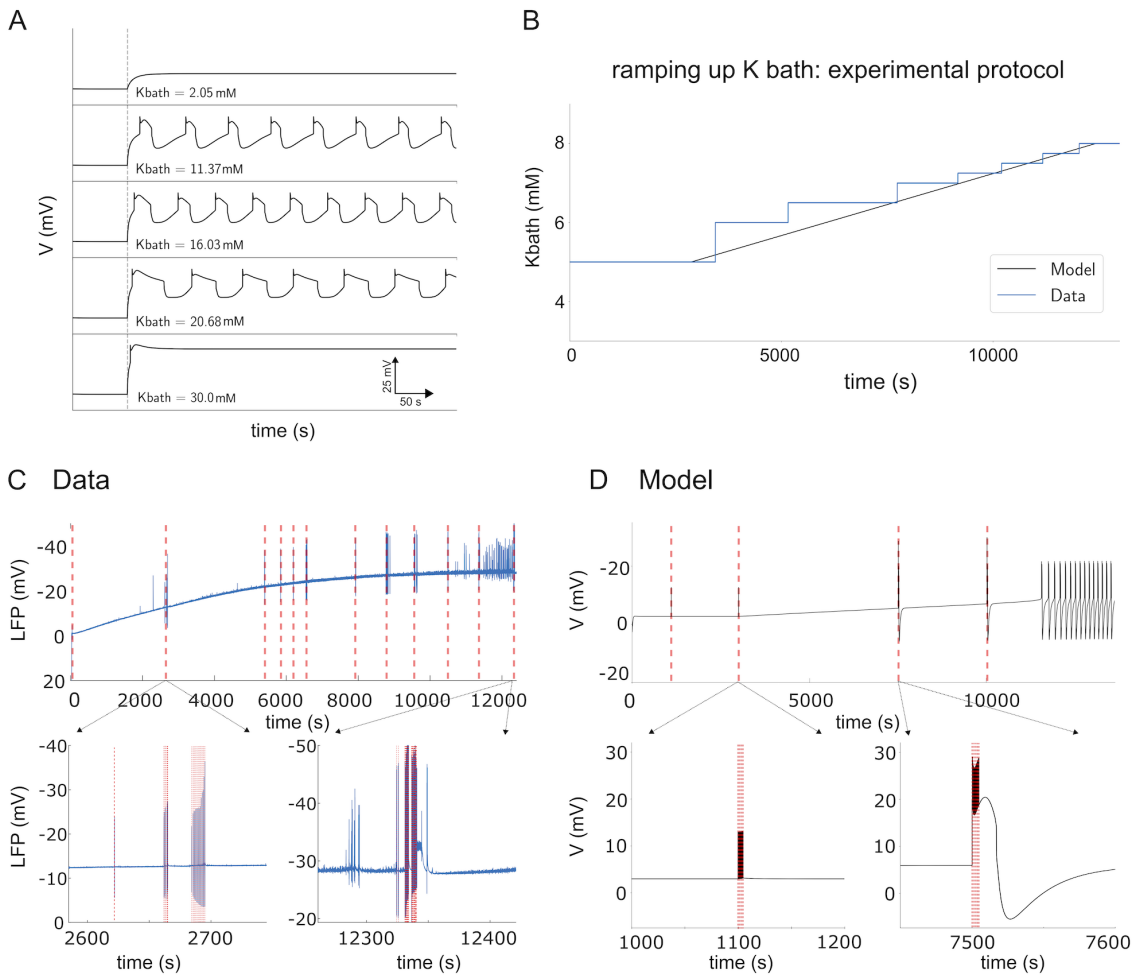

Fig. 2. Highlighting the effect of K_{bath} on the modified Epileptor-2 model compared to the data. (A) Time series of the model for different values of K_{bath}. (B) Superposition of the experimental protocol of sequential addition of potassium performed in the medium containing the slices, with the simulated slow addition protocol. The red vertical dashed lines correspond to the moment when the model is stimulated with a single spike of $A = 15$mA. (C) Effect of the same experimental protocol: the blue time series corresponds to the membrane potential, and the red one to the moment when the experimentalists stimulated the slice. (D) Effect of the slow addition protocol on the model. For panel (C) and (D), zooms on the time series at the moment of the stimulation effect are provided. For the specific parameter, see the Slice M0 in Table 3.

Model predictions regarding optimal parameters and the mechanism of the anti-seizure effect. In order to understand the mechanism behind the anti-seizure effect, we first investigate the optimal stimulation parameters — timing, duration, and amplitude — that maximize it. If the stimulation causes a new seizure, then this is considered the end of the ISI, even as the stimulation continues.

We portray the changes to the ISI in three heatmaps in Fig. 4. In panel A, we plot the effect of amplitude and onset time while keeping the stimulation duration fixed at 50 s. When the amplitude is low, e.g., $A = 0.5$mA, the ISI does not change significantly. When the amplitude increases from 2.5mA to 12.5mA, the stimulation reduces the ISI. However, when the amplitude exceeds 15mA and the onset time is 16s or less, the stimulation increases the ISI by 40% to 60% compared to the unperturbed ISI. If the stimulation onset occurs too late (17s or more), then the stimulation creates a new seizure immediately. We can speak here of a critical point for the stimulation amplitude and stimulation onset. In Fig. 4.B, we plot some corresponding time series that are around this critical point. In panels B.1, 2 and 4, the LFES causes premature seizures. In Fig. 4.B.3, stimulation effectively delays the next seizure and pushes the system onto a new forced equilibrium during stimulation. One can also observe that in panel B.4, the LFES does indeed induce

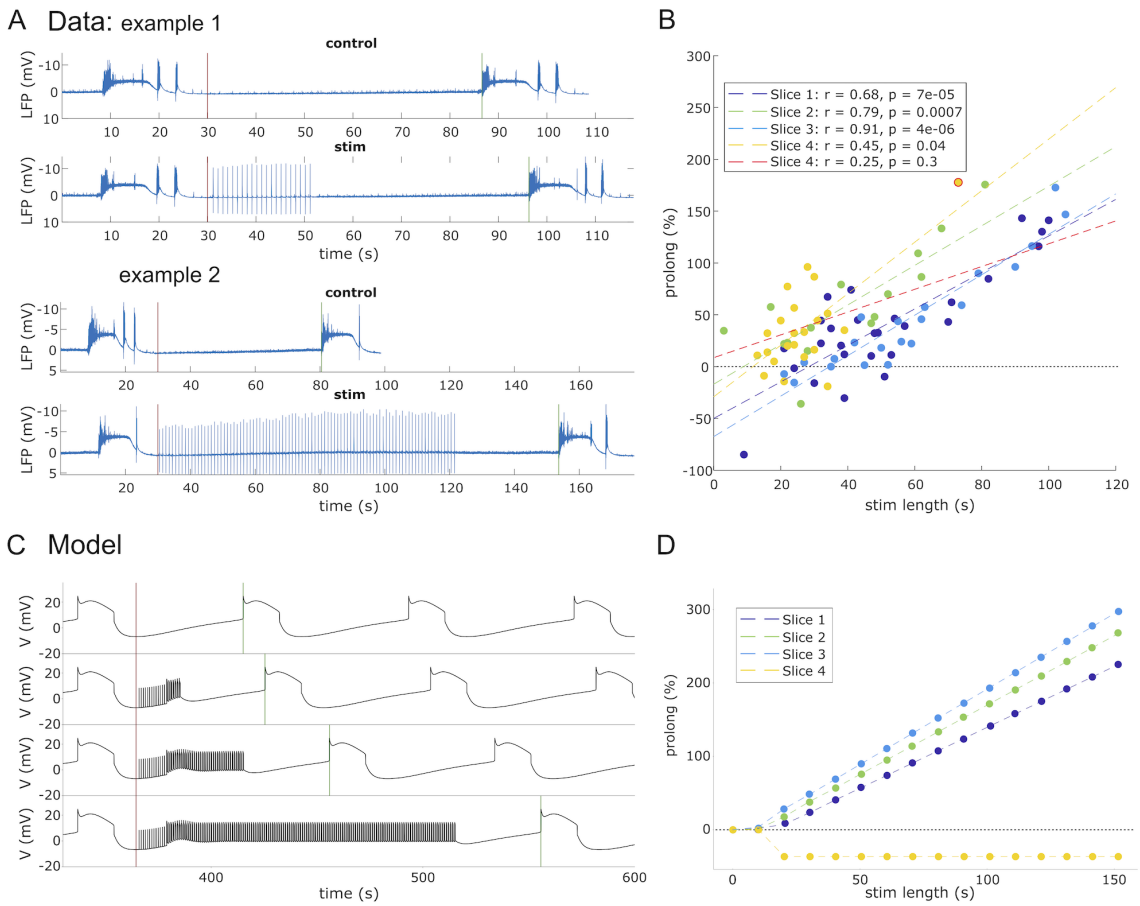

Fig. 3. LFES-induced delay phenomena observed from the data and from the model. (A) Time series from experimental data. The beginning of the ISI is marked by a red vertical line, and this end with the green one. (B) Seizure delay correlation with stimulation length from experimental data, as assessed via Spearman correlation. Seizure delay measured as ISI prolongation (percent change of stimulated ISI relative to control ISI). A Wilcoxon signed-rank test is performed to compare the difference of duration between control and stimulated ISI. Each dashed line is a linear regression fit. For Slice 4, two scenarios are proposed: one with the whole data (yellow dashed line), and one without outlier (red dashed line). The outlier is circled in red. (C) Time series of the simulated model for different stimulation length. For the specific parameter, see the Slice M0 in Table 3. (D) Seizure delay correlation with stimulation length for the Slice 1 to 4 models. For the specific parameters for each slice, see Table 3.

a premature seizure, however unlike panels B.1 and 2 where the stimulation amplitude is not high enough to delay subsequent seizures, what follows the first premature seizure is the beginning of a delay process. This implies that even if the stimulation starts too late and triggers an earlier seizure it can delay the next seizure if the amplitude is high enough.

In Fig. 4.C, we plot the effect of stimulation length and stimulation onset on the ISI, and we observe again the critical value for the stimulation onset. Below this value, the ISI increases linearly with the stimulation length. Note that stimulation with shorter lengths than the one presented in Fig. 4.C will not have a considerable delay effect on ISI. In Fig. 4.D, we plot the effect of stimulation length and stimulation amplitude on the ISI. Again, when the amplitude is above the critical value, the delay is linearly related to stimulation length (see also Fig. 3.D).

Note that our experimental dataset was not sufficient to validate the model predictions regarding optimal parameters. Stimulation amplitude information was not available. Moreover, the stimulation onset time with regard to last seizure offset time varied only between -4.8 and 7.3 seconds with a median of 1.2 seconds (see Supplemental Material S3).

Having identified the critical thresholds for each stimulation parameter, we next aim to elucidate the biological processes underlying the effects of LFES. To achieve this, we analyze the model time series by mapping them onto the Na-K phase plane. To interpret this representa-

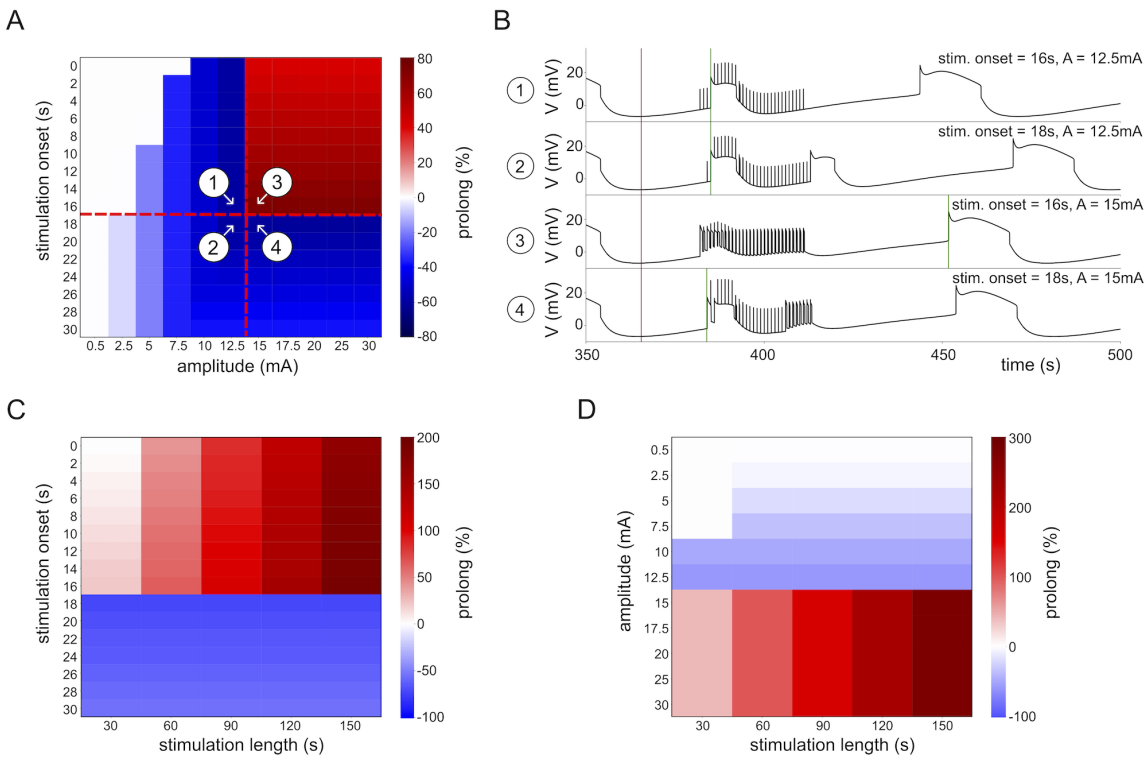

Fig. 4. Seizure delay as a function of three variables: the amplitude of the signal (mA), the stimulation onset after the end of the first seizure (s), and the length of the LFES (s). (A) "amplitude vs onset" with the stimulation length fixed at 25s, (B) Time series numbered from 1 to 4 which are present as a support to understand what is happening around the critical point in (A), (C) "stimulation length vs onset" with the amplitude fixed at 30mA, and (D) "stimulation length vs amplitude" with no onset. For the specific parameter, see the Slice M0 in Table 3.

tion, we highlight the stimulation threshold and employ a bifurcation diagram to delineate the distinct dynamical regimes—namely, ictal and interictal states. This approach allows us to assess whether LFES effectively drives the system away from the ictal into the interictal region.

Fig. 5.A focuses on a time series of the membrane potential from the model, Na/K concentrations, firing rate, and electrical current induced by Na-K pumps, for the case where the LFES is active for 150s. The stimulation sends the system into a regime where the Na-K pump is active (Na: $25.4 - 25.8$mM, K: $3.4 - 3.7$mM). A stimulation pulse causes an instantaneous increase of both Na and K concentration. Then, the active Na-K pump slowly lowers both again. This requires sufficiently strong Na-K pump activity, otherwise the mechanism is likely to fail. This explains why stimulation that occurs too soon after the previous seizure is ineffective in delaying or suppressing the next seizure: the K concentration is still too low and the Na-K pump is inactive. Only when the K concentration is sufficiently high (above ≈ 2.5mM), the mechanism starts working. Conversely, if the stimulation happens too late, the Na concentration is already too low (below$\approx$ 20mM) for the Na-K pumps to be active (see Fig. 4.B, lower panels), and the stimulation ultimately leads to the premature triggering of the seizure.

We now characterize the effects produced by LFES in greater detail. We first focus on the $\{[K^+]_o, [Na^+]_i, V\}$ bifurcation diagram obtained from Eq. Eq. (7) (S-shaped, colored surface in Fig. 4.B), which is superimposed with the trajectory of a solution of the model Eq. Eq. (1) in the absence of stimulation (arrowed black curve). Superimposing these two representations allows us to break down the different regions of the bifurcation diagram: when the black trajectory is in the region with low values of membrane potential V, i.e. the red part of the surface, then it is the interictal region. When the curve approaches the LP_1 bifurcation point, then the trajectory jumps to the blue surface where the values of the membrane potential are high, which represents the ictal phase. Then the curve jumps back down at the HB_1 bifurcation point. This abrupt jump is due to a periodic branch which emerges from HB_1, forming a direct homoclinic connection to the S-shaped surface. For clarity,

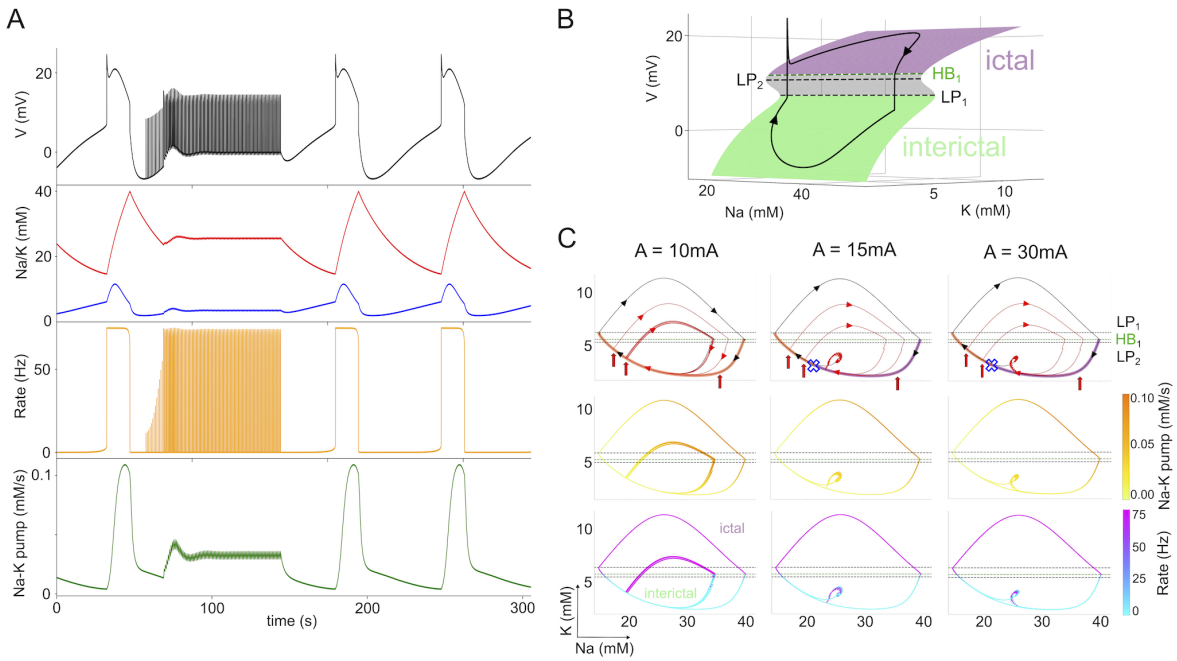

Fig. 5. Deciphering the biological mechanisms underlying LFES. (A) Time series demonstrating seizure delay in response to LFES. (B) 3D $\{[K^+]_o, [Na^+]_i, V\}$ bifurcation diagram obtained from the fast-subsystem (Eq. Eq. (7)), overlaid with a non-stimulated solution obtained from Eq. Eq. (1) (black arrowed curve). For the superposition to be in perfect adequacy, we impose $\varepsilon = 0.003$ parameter in front of the equation of $[K^+]$ and $[Na^+]$, in such a way, they are slower and follow the bifurcation structure. The stable states are the green and purple surface, which refer respectively to the inter-ictal region and the ictal region. The grey surface represents the unstable states. HB denotes Hopf bifurcation, and LP, fold bifurcation point. (C) Effect of our protocol on Eq. Eq. (1) represented on a $\{[Na]^+, [K]^+\}$ phase plane respectively for $A = 10, 15,$ and 30 mA by a stimulated trajectories (arrowed curves), and colormaps of the activity of Na-K pumps, and the firing rate. The start of each stimulation is represented by a vertical red arrow, and last 150s. Trajectories with LFES are plotted in red, trajectories without LFES are plotted in black. The trajectories highlighted in orange or purple indicates where LFES respectively induces an earlier seizure or delays its onset. The blue cross represents the critical point up to which a stimulation causes a delay, as obtained. For the specific parameter, see the Slice M0 in Table 3.

we have omitted the periodic branch in Fig. 4.B, which is further elaborated on in Supplemental Material S4. LP_1 can be regarded as the potassium threshold for which the model produces a seizure if it is exceeded. The grey colored surface corresponds to the unstable states of the system that separate the basins of attraction of the ictal and interictal states.

Having established the different regions, in Fig. 5.C we study the solutions of the model subjected to LFES in the phase plane $\{[K^+]_o, [Na^+]_i\}$, indicating the threshold values obtained in Fig. 5.B (HB_1, LP_1, LP_2) by horizontal lines for better readability. The half-planes below LP_2 and above LP_1 in Fig. 5.C belong to the interictal and the ictal region, respectively. There is a hysteresis effect due to the coexistence of the ictal and interictal regime between LP_1 and LP_2. If a trajectory approaches this interval from the interictal regime (below LP_2), then it remains in the interictal regime; and conversely, if it approaches this interval from the ictal regime (above LP_1), then it will remain in the ictal regime. In the top panels of Fig. 5.C, we plot several trajectories with different stimulation onsets (indicated by the dots of different colors). The blue cross indicates the critical stimulation onset established in Fig. 4. For any stimulation before this critical point, the LFES is effective, otherwise, it causes a premature seizure. For the case $A = 10$mA, the stimulation pushes the system onto a smaller limit cycle (compared to the unperturbed system) that passes through the thresholds. Thus, for any stimulation below the critical stimulation amplitude, seizures are shorter with smaller amplitudes, and shorter ISIs. When $A = 15$mA, for any stimulation arriving before the critical point of stimulation onset, the system stabilizes on a smaller limit cycle. This limit cycle is also observable in the case $A = 30$mA. Since these limit cycles no longer pass through the LP_1 point, they are no longer associated with seizure behavior, but instead, keep the system locked in a subpart of the interictal domain. These results corroborate our observations in Fig. 4, and further suggest that the stronger the stimulation (above $A = 15$mA), the faster is the stabilization at this new stationary cycle.

In Fig. 4, we predicted that if we choose the right am-

plitude to induce a delay but stimulate too late, then we induce a single transient seizure before converging to the delay process. In Fig. 5.C, with 15mA and 30mA, we can clearly see this process. The solution passes through the seizure domain once, before converging to the new attractor. This implies that the onset threshold relative to the last seizure only acts as a threshold for the initial conditions of the LFES. In fact, for any LFES above 15mA, the delay appears with or without a single transient seizure.

The second and third row of panels in Fig. 5.C show the trajectories obtained from the same simulations as the first row, but with color coding of the current induced by the Na-K pump I_{pump}, and the firing rate υ_i, respectively. We can observe the activation and deactivation of the Na-K pump during a seizure: initially, the intracellular sodium concentration is low, and the pumps have very low activity. During the seizure, at the peak of activity, the pump reactivates due to the accumulated intracellular sodium, and decreases the extracellular potassium concentrations, which brings the neuronal population back to the baseline. When stimulating with $A = 10$mA, this process also occurs during the appearance of the premature seizure. When the amplitude is large enough to delay seizures, the system converges onto a new attractor where the Na-K pump becomes increasingly active compared to the resting state without stimulation. The firing rate υ_i provides an indication of the effect of the stimulation protocol on the model. During the interictal phase, the firing rate is close to zero, whereas in the ictal phase it is close to the maximum υ_{max}. When LFES is applied to the system, the firing rate shows a burst-like response to the stimulation pulses. However, the amplitude of these bursts only reaches its maximum when the stimulation is effective in delaying the subsequent seizure. The bursts of firing activity increase K and Na concentrations, which is counteracted by the Na-K pumps, thus establishing a new attractor state.

In summary, this analysis highlights the critical role of the Na-K pump in the processes induced by LFES, stabilizing ionic concentrations at relatively low values. We demonstrate that the observed phenomenon is not associated with epileptic activity. Instead, it represents an interictal dynamic that maintains the system at a safe distance from the seizure transition.

Discussion

In this study, we provide a deeper understanding of brain stimulation as a treatment for epilepsy by means of a modified version of the Epileptor-2 model (25). This work bridges the gap between experimental findings and theoretical insights, providing a deeper understanding of how LFES interacts with seizure dynamics at a mechanistic level. Leveraging experimental data from hippocampal rat slices under high-potassium condition, we reproduce key features of seizure-like events, such as their onset, duration, and ISIs, while also accounting for the variability observed across individual slices. The model not only recapitulates these experimental findings, but also offers novel insights into how LFES modulates ion dynamics, particularly through its impact on the Na-K pump. This mechanism stabilizes ionic concentrations, thereby delaying seizure onset, maintaining the system in an interictal state. By systematically exploring the onset, amplitude, and duration of LFES, we identify optimal stimulation parameters maximizing its anti-seizure effects without inadvertently triggering epileptic activity.

In the original Epileptor-2 model, the addition of LFES in the inter-seizure interval had either no effect, or caused premature seizures for any amplitude (see Supplemental Material S5). We therefore applied some modifications necessary to account for the seizure delay observed in the data. These modifications involve a smoother sigmoid firing rate function, and new dynamics for the inhibitory neuronal population. The latter was considered to balance the dynamics of the excitatory population in the original model, which we replaced by an inhibitory population providing background inhibition at a constant firing rate (27). However, in Supplemental Material S6, we demonstrate that after removing inhibition completely from the modified Epileptor-2, the model still produces seizures, and LFES is effective in delaying them. This implies that the inhibitory population in our model is not crucial for the emergence of seizures or their delay.

There are some differences between the experimental protocol and the model setup. First, our ability to fit the model to the data is limited by the nature of the LFP, which is generated by multiple different processes (40, 41) that are difficult to disentangle, especially in terms of the amplitude of the signal. Therefore, while the data represent the LFP measured in the extracellular medium, the model describes the average membrane potential of the pyramidal cells. To obtain a match between the data and model, we aligned the temporal features of the model output with the experimentally observed seizure dynamics, such as seizure length and ISI, ignoring the amplitude of the signal. To further demonstrate the model's validity, we reproduced experimental pro-

tocols in model simulations, such as the effect of stepwise increase of potassium concentration in the ACSF (Fig. 2B). Second, in the experiment the stimulation was performed on the Schaffer collaterals coming from the CA3 region extending towards CA1. This stimulation likely elicits spike volleys in the axons traveling to CA1, where they generate postsynaptic potentials at the excitatory population. The relationship between the amplitude of the electric field and the number of elicited spikes in the Schaffer collaterals (and the resulting postsynaptic potentials in CA1) is likely nonlinear. It is reasonable to assume that stimulation leads to a binary response at the level of single axons, where the electric field is either strong enough to elicit a spike, or too weak to do so. Because larger axons activate at smaller field strengths than smaller axons (42), the morphological heterogeneity of axons may result in a more graded response, at least in a narrow range of electric field strengths. Since the exact relationship between the electric field strength and the resulting PSPs in CA1 is unknown, we decided to directly use the amplitude of the postsynaptic current as model parameter.

We further examined optimal LFES in terms of stimulation onset, duration and amplitude. We identified critical values for onset and amplitude: if the onset occurs too late, or the amplitude is too low, then even a single stimulation pulse has an adverse effect and triggers a premature seizure. For onset times before the critical time point and amplitudes above the critical intensity, their exact values do not play a role in the delaying effect. However, the duration of the stimulation is a crucial parameter, with which the relative delay of the seizure increases linearly, which is corroborated by our experimental results. Thus, the LFES applied to the model led to the emergence of a new small periodic equilibrium during stimulation, if applied at the right time and amplitude. Given our discussion in the previous paragraph, in the experimental setup the critical stimulation amplitude is likely mediated by the structural properties of the Schaffer collaterals, and therefore, doesn't directly relate to the stimulation amplitude used in the model.

Finally, the mathematical model allowed us to analyse the processes underlying the emergence of seizures and the seizure delay due to LFES. Seizures in the Epileptor-2 model occur periodically, driven by intracellular sodium and extracellular potassium concentration dynamics. During the interictal period, intracellular sodium decreases and extracellular potassium increases. The latter happens due to diffusion of potassium from the potassium-enriched ACSF perfusing the slice. Due to the accumulation of extracellular potassium, the system eventually switches to the ictal state, which is characterized by high extracellular potassium, the depolarisation of the membrane, and an increase in the firing rate. The increased firing rate leads to an accumulation of intracellular sodium throughout the ictal phase, and a further accumulation of extracellular potassium in the first stage of the seizure. In the second stage of the seizure, when both sodium and potassium concentrations are sufficiently high, the sodium-potassium pumps activate and decreasing extracellular potassium (but barely affecting the sodium concentration, due to the volume ratio parameter), eventually lowering the membrane potential sufficiently for the system to reverse to the interictal phase. Thus, it appears that Na-K pumps are crucial for the termination of ictal phase because they lower the extracellular potassium concentration. During the interictal phase, however, the activity of the Na-K pumps is not enough to compensate for the potassium concentration increase due to the diffusion from the high-potassium ACSF. There is a time window during the interictal phase, when the system is in, or close to, the regime where sodium-potassium pumps are active. The stimulation protocol causes the neurons to fire and, thus, increases both sodium and potassium concentrations. The system then moves to a state in which the activity of the Na-K pump is counterbalanced by the stimulation, which is sufficient to suppress further increases in the extracellular potassium concentration and, thus, prevents spontaneous seizure occurrence.

The crucial role played by Na-K-pumps in seizure termination as well as for the ionic balance in general, is supported by experimental studies (43–48). Blocking Na-K-pumps with ouabain elicits long-lasting seizures in otherwise healthy tissue (49). Furthermore, inherited and acquired sodium or potassium-related channelopathies (50, 51) and genetic Na-K-pump dysfunctions can cause epilepsy (52). Anti-seizure medications aimed at restoring normal Na-K-ATPase function might alleviate symptoms in patients with pump-related mutations (44, 50). This suggests, in line with the findings of our study, that Na-K-pump-related mechanisms could also be a viable target for stimulation treatment.

Other modeling studies investigating the effects of LFES in epilepsy have used the same theoretical framework but focus on the role of presynaptic $GABA_B$ receptors (12). In contrast, (20) adopt a theoretical framework based on phase response analysis of planar relaxation oscillators and the Epileptor model (53), exploring how the slow vector field influences seizure emergence and re-

sponses to perturbations that can be likened to LFES. The Epileptor described in (20) is a phenomenological model that does not have a biophysical variable to understand the mechanisms underlying stimulation; however, it provides a broader mathematical foundation for understanding perturbation effects in epileptic models. This work shows that it is possible to obtain a delaying effect with small-amplitude stimulation close to the next seizure, contradicting the notion of an optimal stimulation window in our study. Together, they highlight the interplay between theoretical modeling and experimental validation, reinforcing the necessity of both perspectives in refining treatment strategies for epilepsy.

Conclusion

In conclusion, this work provides a significant advancement in understanding the effects of LFES on seizure dynamics by modifying the Epileptor-2 model to better align with experimental data. By integrating parameters from in vitro hippocampal recordings, the model uncovers a key mechanism through which LFES modulates the Na-K pump, stabilizing ionic concentrations and delaying seizure onset. The identification of critical amplitude and duration parameters for LFES offers new insights into optimizing this therapeutic approach. These findings bridge the gap between theoretical modeling and experimentation, providing a robust framework for refining stimulation strategies in epilepsy treatment.

ACKNOWLEDGEMENTS

This work was supported by ERDF-Project Brain dynamics, No. CZ.02.01.01/00/22_008/0004643, by project nr. LX22NPO5107 (MEYS): Financed by EU – Next Generation EU, Czech Science Foundation (21-17564S), a Lumina-Quaeruntur fellowship (LQ100302301) by the Czech Academy of Sciences (awarded to HS), and the long-term strategic development financing of the Institute of Computer Science (RVO:67985807) of the Czech Academy of Sciences, and Charles University grant PRIMUS/23/MED/011.

We would like to thank Thomas R. Knösche for valuable discussions.

Bibliography

1. Kirsten M. Fiest, Khara M. Sauro, Samuel Wiebe, Scott B. Patten, Churl-Su Kwon, Jonathan Dykeman, Tamara Pringsheim, Diane L. Lorenzetti, and Nathalie Jetté. Prevalence and incidence of epilepsy. *Neurology*, 88(3):296–303, 2017. doi: 10.1212/WNL.0000000000003509.
2. Ettore Beghi. The Epidemiology of Epilepsy. *Neuroepidemiology*, 54(2):185–191, 12 2019. ISSN 0251-5350. doi: 10.1159/000503831.
3. Meir Bialer and H White. Key factors in the discovery and development of new antiepileptic drugs. *Nature reviews. Drug discovery*, 9:68–82, 01 2010. doi: 10.1038/nrd2997.
4. Felix Rosenow and Hans Lüders. Presurgical evaluation of epilepsy. *Brain*, 124(9):1683–1700, September 2001. ISSN 0006-8950. doi: 10.1093/brain/124.9.1683.
5. Santoshi Billakota, Orrin Devinsky, and Kyung-Wha Kim. Why we urgently need improved epilepsy therapies for adult patients. *Neuropharmacology*, 170:107855, June 2020. ISSN 00283908. doi: 10.1016/j.neuropharm.2019.107855.
6. Yicong Lin and Yuping Wang. Neurostimulation as a promising epilepsy therapy. *Epilepsia Open*, 2(4):371–387, 2017. ISSN 2470-9239. doi: 10.1002/epi4.12070.
7. Robert S Fisher and Ana Luisa Velasco. Electrical brain stimulation for epilepsy. *Nature Reviews Neurology*, 10(5):261–270, 2014.
8. Yujiang Wang, Frances Hutchings, and Marcus Kaiser. Computational modeling of neurostimulation in brain diseases. In *Progress in Brain Research*, volume 222, pages 191–228. Elsevier, 2015. ISBN 978-0-444-63546-4. doi: 10.1016/bs.pbr.2015.06.012.
9. Isa Dallmer-Zerbe, Premysl Jiruska, and Jaroslav Hlinka. Personalized dynamic network models of the human brain as a future tool for planning and optimizing epilepsy therapy. *Epilepsia*, page epi.17690, July 2023. ISSN 0013-9580, 1528-1167. doi: 10.1111/epi.17690.
10. Fabrice Wendling, Pascal Benquet, Fabrice Bartolomei, and V. K. Jirsa. Computational models of epileptiform activity. *Journal of Neuroscience Methods*, 260:233–251, February 2016. ISSN 01650270. doi: 10.1016/j.jneumeth.2015.03.027.
11. Kara Buehrer Kile, Nan Tian, and Dominique M Durand. Low frequency stimulation decreases seizure activity in a mutation model of epilepsy. *Epilepsia*, 51(9):1745–1753, 2010.
12. Elena Y. Smirnova, Anton V. Chizhov, and Aleksey V. Zaitsev. Presynaptic GABAB receptors underlie the antiepileptic effect of low-frequency electrical stimulation in the 4-aminopyridine model of epilepsy in brain slices of young rats. *Brain Stimulation*, 13(5):1387–1395, 2020. ISSN 1935-861X. doi: https://doi.org/10.1016/j.brs.2020.07.013.
13. Mohamad Z Koubeissi, Emine Kahriman, Tanvir U Syed, Jonathan Miller, and Dominique M Durand. Low-frequency electrical stimulation of a fiber tract in temporal lobe epilepsy. *Annals of neurology*, 74(2):223–231, 2013.
14. Junichi Yamamoto, Akio Ikeda, Takeshi Satow, Kazuhide Takeshita, Motohiro Takayama, Masao Matsuhashi, Riki Matsumoto, Shinji Ohara, Nobuhiro Mikuni, Jun Takahashi, et al. Low-frequency electric cortical stimulation has an inhibitory effect on epileptic focus in mesial temporal lobe epilepsy. *Epilepsia*, 43(5):491–495, 2002.
15. Colette Boëx, Serge Vulliémoz, Laurent Spinelli, Claudio Pollo, and Margitta Seeck. High and low frequency electrical stimulation in non-lesional temporal lobe epilepsy. *Seizure*, 16(8):664–669, 2007.
16. Lara M Schrader, John M Stern, Charles L Wilson, Tony A Fields, Noriko Salamon, Marc R Nuwer, Paul M Vespa, and Itzhak Fried. Low frequency electrical stimulation through subdural electrodes in a case of refractory status epilepticus. *Clinical neurophysiology*, 117(4):781–788, 2006.
17. Michael CH Li and Mark J Cook. Deep brain stimulation for drug-resistant epilepsy. *Epilepsia*, 59(2):273–290, 2018.
18. Clement Hamani, Danielle Andrade, Mojgan Hodaie, Richard Wennberg, and Andres Lozano. Deep brain stimulation for the treatment of epilepsy. *International journal of neural systems*, 19(03):213–226, 2009.
19. Wei-Chih Chang, Jan Kudlacek, Jaroslav Hlinka, Jan Chvojka, Michal Hadrava, Vojtech Kumpost, Andrew D. Powell, Radek Janca, Matias I. Maturana, Philippa J. Karoly, Dean R. Freestone, Mark J. Cook, Milan Palus, Jakub Otahal, John G. R. Jefferys, and Premysl Jiruska. Loss of neuronal network resilience precedes seizures and determines the ictogenic nature of interictal synaptic perturbations. *Nat Neurosci*, 21(12):1742–1752, December 2018. ISSN 1097-6256, 1546-1726. doi: 10.1038/s41593-018-0278-y.
20. Alberto Pérez-Cervera and Jaroslav Hlinka. Perturbations both trigger and delay seizures due to generic properties of slow-fast relaxation oscillators. *PLOS Computational Biology*, 17(3):1–25, 03 2021. doi: 10.1371/journal.pcbi.1008521.
21. Faten Mina, Pascal Benquet, Anca Pasnicu, Arnaud Biraben, and Fabrice Wendling. Modulation of epileptic activity by deep brain stimulation: a model-based study of frequency-dependent effects. *Frontiers in computational neuroscience*, 7:94, 2013.
22. Hossein Sohanian Haghighi and Amir HD Markazi. Control of epileptic seizures by electrical stimulation: a model-based study. *Biomedical Physics & Engineering Express*, 7(6):065009, 2021.
23. Gagan Acharya, Kathryn A Davis, and Erfan Nozari. Predictive modeling of evoked intracranial eeg response to medial temporal lobe stimulation in patients with epilepsy. *Communications Biology*, 7(1):1210, 2024.
24. Arian Ashourvan, Sérgio Pequito, Ankit N Khambhati, Fadi Mikhail, Steven N Baldassano, Kathryn A Davis, Timothy H Lucas, Jean M Vettel, Brian Litt, George J Pappas, et al. Model-based design for seizure control by stimulation. *Journal of neural engineering*, 17(2):026009, 2020.
25. Anton V. Chizhov, Artyom V. Zefirov, Dmitry V. Amakhin, Elena Yu. Smirnova, and Aleksey V. Zaitsev. Minimal model of interictal and ictal discharges "epileptor-2". *PLOS Computational Biology*, 14(5):1–25, 05 2018. doi: 10.1371/journal.pcbi.1006186.
26. Jeffry S Isaacson and Massimo Scanziani. How inhibition shapes cortical activity. *Neuron*, 72(2):231–243, 2011.
27. Christoph Börgers, Martin Krupa, and Stan Gielen. The response of a classical hodgkin–huxley neuron to an inhibitory input pulse. *Journal of computational neuroscience*, 28:509–26, 04 2010. doi: 10.1007/s10827-010-0233-8.
28. John R Cressman, Ghanim Ullah, Jokubas Ziburkus, Steven J Schiff, and Ernest Barreto. The influence of sodium and potassium dynamics on excitability, seizures, and the stability of persistent states: I. single neuron dynamics. *Journal of computational neuroscience*, 26:159–170, 2009.
29. Imre Vida, Marlene Bartos, and Peter Jonas. Shunting inhibition improves robust-

ness of gamma oscillations in hippocampal interneuron networks by homogenizing firing rates. *Neuron*, 49(1):107–117, 2006.
30. Ruben A Tikidji-Hamburyan and Carmen C Canavier. Shunting inhibition improves synchronization in heterogeneous inhibitory interneuronal networks with type 1 excitability whereas hyperpolarizing inhibition is better for type 2 excitability. *eneuro*, 7 (3), 2020.
31. Marom Bikson, Philip J Hahn, John E Fox, and John GR Jefferys. Depolarization block of neurons during maintenance of electrographic seizures. *Journal of Neurophysiology*, 90(4):2402–2408, 2003.
32. György Buzsáki. Large-scale recording of neuronal ensembles. *Nature neuroscience*, 7(5):446–451, 2004.
33. Gianmaria Maccaferri and Raymond Dingledine. Control of feedforward dendritic inhibition by nmda receptor-dependent spike timing in hippocampal interneurons. *Journal of Neuroscience*, 22(13):5462–5472, 2002.
34. Jennifer A Kim and Barry W Connors. High temperatures alter physiological properties of pyramidal cells and inhibitory interneurons in hippocampus. *Frontiers in cellular neuroscience*, 6:27, 2012.
35. Joseph V Raimondo, Richard J Burman, Arieh A Katz, and Colin J Akerman. Ion dynamics during seizures. *Frontiers in cellular neuroscience*, 9:419, 2015.
36. John D Mayer and Peter Salovey. *Mayer-Salovery-Caruso emotional intelligence test*. Multi-Health Systems Incorporated Toronto, 2007.
37. Andrea O Rossetti, Giancarlo Logroscino, and Edward B Bromfield. Refractory status epilepticus: effect of treatment aggressiveness on prognosis. *Archives of neurology*, 62(11):1698–1702, 2005.
38. M Holtkamp, J Othman, K Buchheim, and H Meierkord. Predictors and prognosis of refractory status epilepticus treated in a neurological intensive care unit. *Journal of Neurology, Neurosurgery & Psychiatry*, 76(4):534–539, 2005.
39. Birgit Frauscher, Fabrice Bartolomei, Maxime O. Baud, Rachel J. Smith, Greg Worrell, and Brian N. Lundstrom. Stimulation to probe, excite, and inhibit the epileptic brain. *Epilepsia*, 64 Suppl 3(Suppl 3):S49–S61, December 2023. ISSN 1528-1167. doi: 10.1111/epi.17640.
40. György Buzsáki, Costas A Anastassiou, and Christof Koch. The origin of extracellular fields and currents—EEG, ECoG, LFP and spikes. *Nature reviews neuroscience*, 13(6):407–420, 2012.
41. Henrik Lindén, Tom Tetzlaff, Tobias C Potjans, Klas H Pettersen, Sonja Grün, Markus Diesmann, and Gaute T Einevoll. Modeling the spatial reach of the LFP. *Neuron*, 72 (5):859–872, 2011.
42. Jessica L Gaines, Kathleen E Finn, Julia P Slopsema, Lane A Heyboer, and Katharine H Polasek. A model of motor and sensory axon activation in the median nerve using surface electrical stimulation. *Journal of computational neuroscience*, 45:29–43, 2018.
43. Morten S Jensen and Yoel Yaari. Role of intrinsic burst firing, potassium accumulation, and electrical coupling in the elevated potassium model of hippocampal epilepsy. *Journal of neurophysiology*, 77(3):1224–1233, 1997.
44. Jinyi Sun, Yang Zheng, Zhong Chen, and Yi Wang. The role of na+-k+-atpase in the epileptic brain. *CNS Neuroscience & Therapeutics*, 28(9):1294–1302, 2022.
45. Alina M Trofimova, Dmitry V Amakhin, Tatyana Y Postnikova, Vasilii S Tiselko, Alexey Alekseev, Elizaveta Podoliak, Valentin I Gordeliy, Anton V Chizhov, and Aleksey V Zaitsev. Light-driven sodium pump as a potential tool for the control of seizures in epilepsy. *Molecular Neurobiology*, 61(7):4691–4704, 2024.
46. Thierry Grisar. Glial and neuronal na+-k+ pump in epilepsy. *Annals of Neurology: Official Journal of the American Neurological Association and the Child Neurology Society*, 16(S1):S128–S134, 1984.
47. T Grisar, D Guillaume, and AV Delgado-Escuet. Contribution of na+, k+-atpase to focal epilepsy: a brief review. *Epilepsy research*, 12(2):141–149, 1992.
48. MICHAEL M Haglund and PHILIP A Schwartzkroin. Role of na-k pump potassium regulation and ipsps in seizures and spreading depression in immature rabbit hippocampal slices. *Journal of neurophysiology*, 63(2):225–239, 1990.
49. Timothy A Pedley, Emil C Zuckermann, and Gilbert H Glaser. Epileptogenic effects of localized ventricular perfusion of ouabain on dorsal hippocampus. *Experimental neurology*, 25(2):207–219, 1969.
50. Carl E Stafstrom. Persistent sodium current and its role in epilepsy. *Epilepsy Currents*, 7(1):15–22, 2007.
51. Rüdiger Köhling and Jakob Wolfart. Potassium channels in epilepsy. *Cold Spring Harbor perspectives in medicine*, 6(5):a022871, 2016.
52. Karl P Schlingmann, Sascha Bandulik, Cherry Mammen, Maja Tarailo-Graovac, Rikke Holm, Matthias Baumann, Jens König, Jessica JY Lee, Britt Drögemöller, Katrin Imminger, et al. Germline de novo mutations in atp1a1 cause renal hypomagnesemia, refractory seizures, and intellectual disability. *The American Journal of Human Genetics*, 103(5):808–816, 2018.
53. Kenza El Houssaini, Christophe Bernard, and Viktor K. Jirsa. The epileptor model: A systematic mathematical analysis linked to the dynamics of seizures, refractory status epilepticus, and depolarization block. *eNeuro*, 7(2), 2020. doi: 10.1523/ENEURO.0485-18.2019.

Supplemental Material 1: Data Analysis - Inter-Seizure-Intervals (ISI)

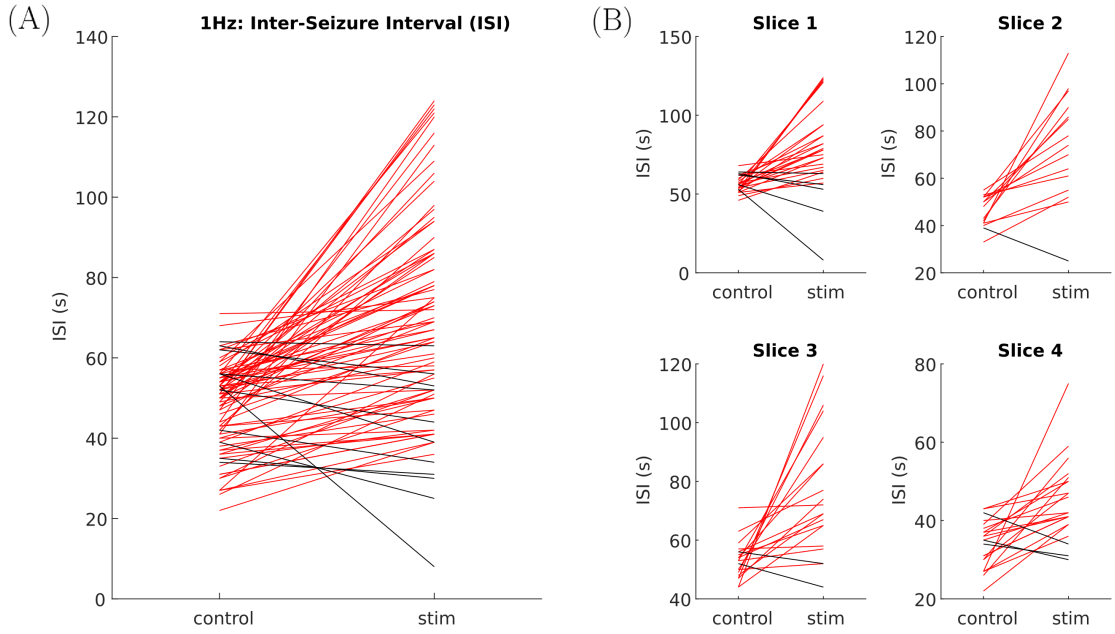

Figure S1: (A) Inter-seizure-interval across slices. Prolonged ISIs under stimulation are marked in red, shortened ISIs in black. Most ISIs are prolonged. (B) Inter-seizure-interval per slice. All slices show the delay effect. Note the variation in slice-specific ISI. The seizure delay (marked in red), as induced by 1 Hz stimulation, is clearly visible on the group level, as well as in the individual slices.

Supplemental Material 2: LFES efficiency regions in Modified Epileptor-2

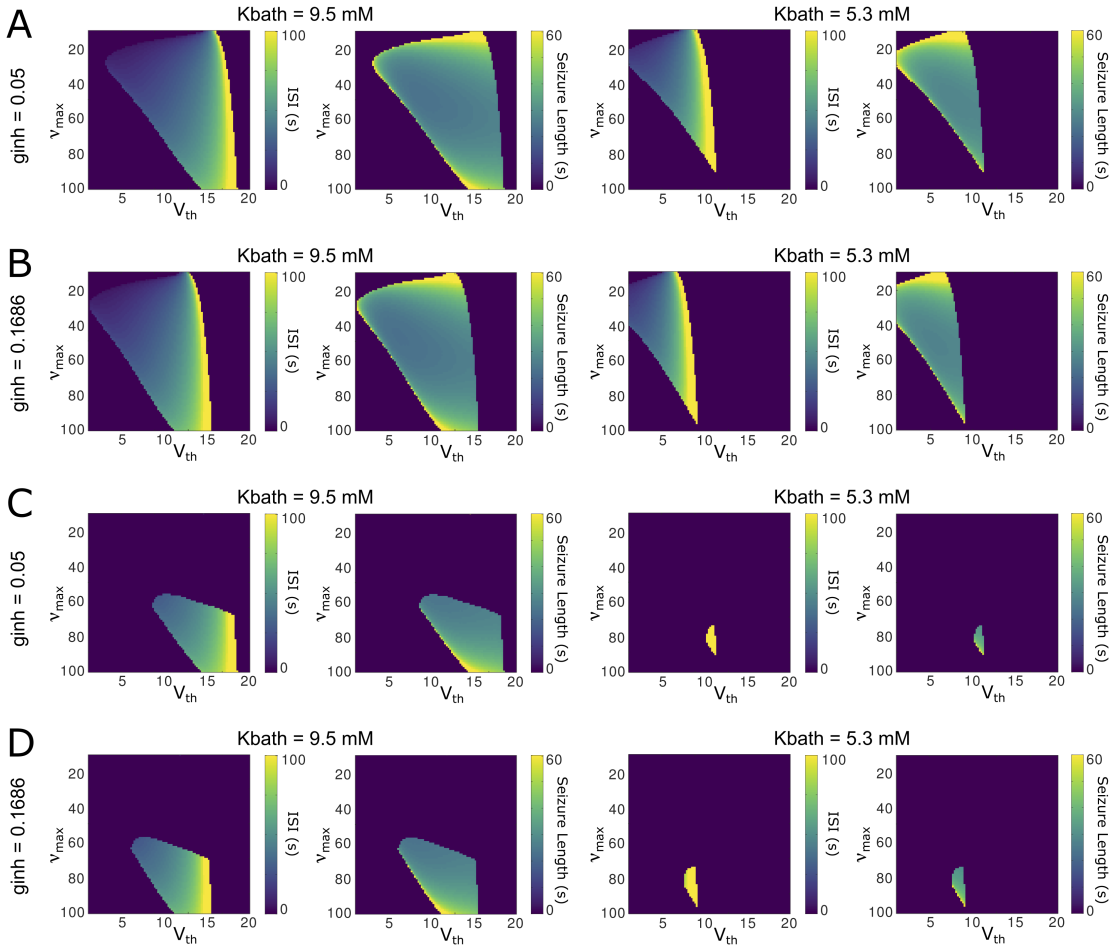

Figure S2: Heatmaps of ISI and seizure duration with respect to the parameters V_{th}, v_{max} and g_{inh}, for Slice 1 ($K_{bath} = 9.5$) and 4 ($K_{bath} = 5.3$). (A-B) Heatmaps for $g_{inh} = 0.1686$ and $g_{inh} = 0.05$ respectively. (C-D) Same activity maps, however, the pixels for which the model exhibits seizures, but where the LFES is not effective have been set to 0. LFES fails to delay seizures in Slice 4 (see Fig 3), prompting an investigation using activity maps to assess the effects of inhibitory current and key parameters on seizure dynamics. These maps reveal how inhibition influences seizure occurrence, duration, and spacing under Slice 1 and 4 conditions. Increasing inhibition shifts the seizure-prone region to higher threshold values, enabling better data fitting for Slice 4 with $g_{inh} = 0.1686$. However, while Slice 1 allows both accurate data fitting and effective LFES, no parameter set achieves this for Slice 4, highlighting limitations in the model's ability to reproduce both seizure dynamics and stimulation effects. For the specific parameters for each slice, see the main result Table 3.

Supplemental Material 3: Data Analysis - Stimulation parameters

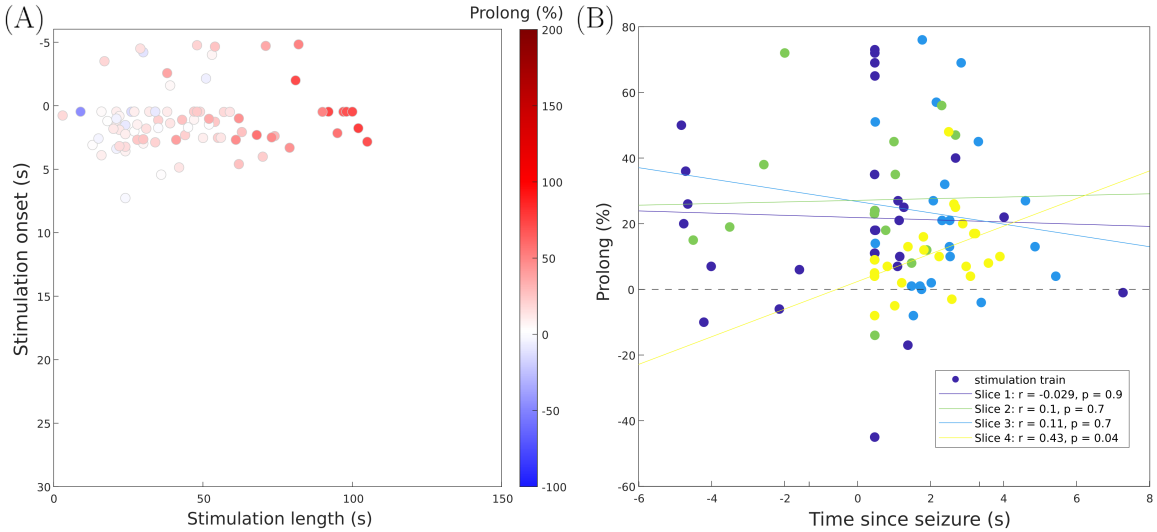

Figure S3: (A) Stimulation onset time expressed as time since last seizure and stimulation length, displayed in accordance with Fig. 4.C of the main manuscript. Most of the parameter space explored in Fig. 4.C was not covered in the experimental dataset. Stimulation onset in the dataset was centered around last seizure offset. For stimulation lenth, the experimental observation matched the model prediction: longer stimulation time led to higher prolongation of the stimulated ISI as compared to the control ISI. (B) Relationship of stimulation parameters and seizure delay in each of the slices (color-coded). For the narrow parameter range explored, stimulation onset time did not seem to correlate with with the seizure delaying effect of LFES. Due to data limitations, a thorough exploration of the parameter space, as for the model in Fig. 4 of the main manuscript, was not possible. Stimulation amplitude was not available. Stimulation onset time varied only in a small range close to previous seizure end in panel (A). In this time window we did not see a significant correlation between seizure delay ("Prolong") and stimulation onset time ("Time since seizure") in panel (B).

Supplemental Material 4: $\{[K^+]_o, V\}$-bifurcation diagram

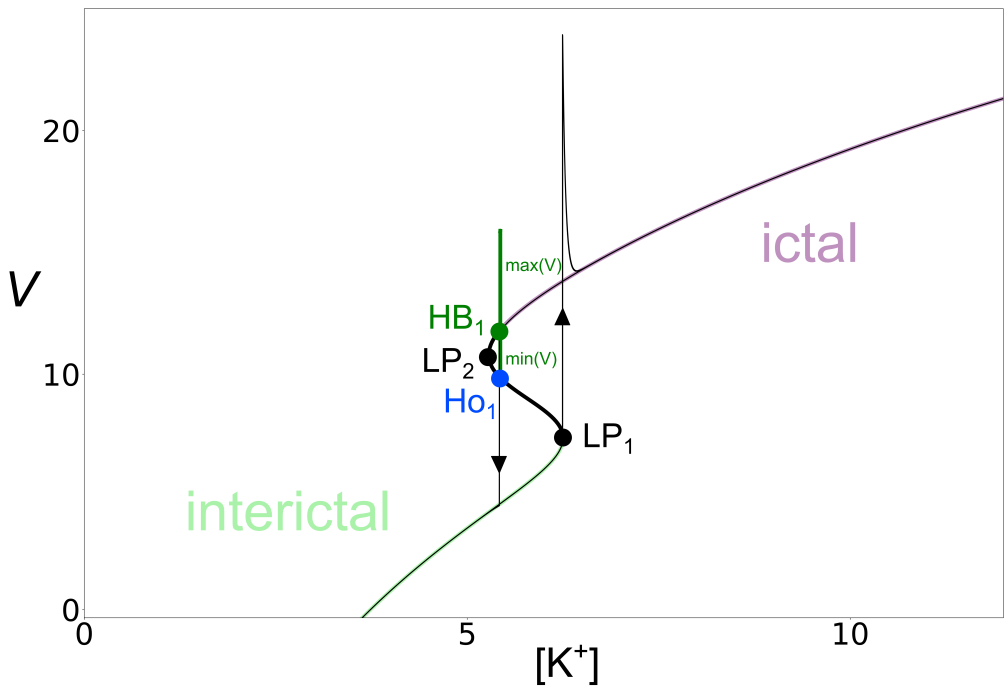

Figure S4: $\{[K^+]_o, V\}$ bifurcation diagram obtained from the fast-subsystem (Eq. Eq. (7)), overlaid with a non-stimulated solution obtained from Eq. Eq. (1) (black arrowed curve). For the superposition to be in perfect adequacy, we impose $\varepsilon = 0.003$ parameter in front of the equation of $[K^+]$, in such a way, they are slower and follow the bifurcation structure. The stable states are the light green and purple curves, which refer respectively to the inter-ictal region and the ictal region. The black curve represents the unstable states. HB denotes Hopf bifurcation, LP, fold bifurcation, and Ho, homoclinc bifurcation. The deep green curve refers to the periodic branch. This figure highlights the periodic branch arising from the Hopf point, and the presence of a homoclinic bifurcation point when it is interrupted in the unstable branch of the S-shaped stationary point curve. The verticality and explosiveness of the periodic branch therefore do not allow the existence of a periodic solution, even with slow trajectories. Thus, the solution that crosses the Hopf point after passing the ictal phase, jumps directly to the interictal phase, passing through the point Ho_1.

Supplemental Material 5: Original Epileptor-2 model study

Parameter	Description	Value
γ	Volume ratio	10
δ_K	Concentration increments at spike for potassium dynamics	0.02 mM
δ_{Na}	Concentration increments at spike for sodium dynamics	0.03 mM
δ_x	Concentration increments at spike for synaptic depression	0.01
K_{bath}	Potassium concentration in the bath	8.5 mM
$[K^+]_{\mathrm{o}}^0$	Initial extracellular potassium concentration	3.0 mM
$[Na^+]_{\mathrm{i}}^0$	Initial intracellular sodium concentration	10.0 mM
τ_K	Time constant for potassium dynamics	10.0 s *
τ_{Na}	Time constant for sodium dynamics	20.0 s *
τ_m	Time constant for membrane potential	0.01 s *
τ_x	Time constant for synaptic depression	2.0 s
ρ	Maximum pump flux	0.2 mM/s *
v_{max}	Maximal rate of the firing rate function	100.0 Hz *
V_{th}	Threshold potential	5.0 mV *
g_{exc}	Conductance of the excitatory population	5.0 *
g_L	Conductance of the leak flux	1.0
g_K	Conductance of the potassium flux	0.5
k_v	Gain of the firing rate function	20mV *

Table S1: Original parameter set for the Epileptor-2 model. The parameters marked with * are different from modified Epileptor-2. The original Epileptor-2 equations are defined in (25).

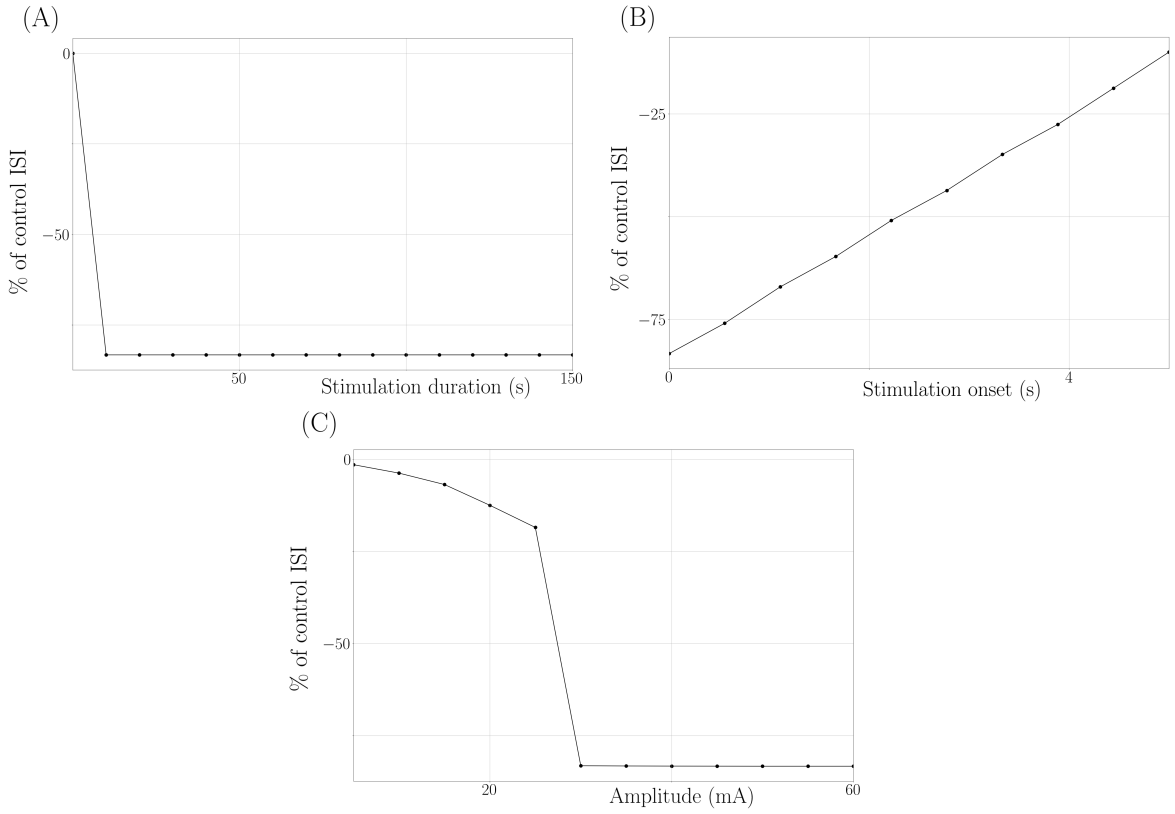

Figure S5: LFES effects on the Epileptor-2 model. Stimulated ISI expressed as a percentage relative to the unstimulated ISI, with respect to (A) stimulation duration (s), (B) stimulation shift (s), and (C) amplitude (mA). Results show that stimulation generally shortens the ISI, with earlier stimulations leading to earlier subsequent seizures, and that increasing amplitude beyond 30mA does not further delay seizure onset. The parameter set is described in Table S1.

Supplemental Material 6: Removing the inhibition dependency

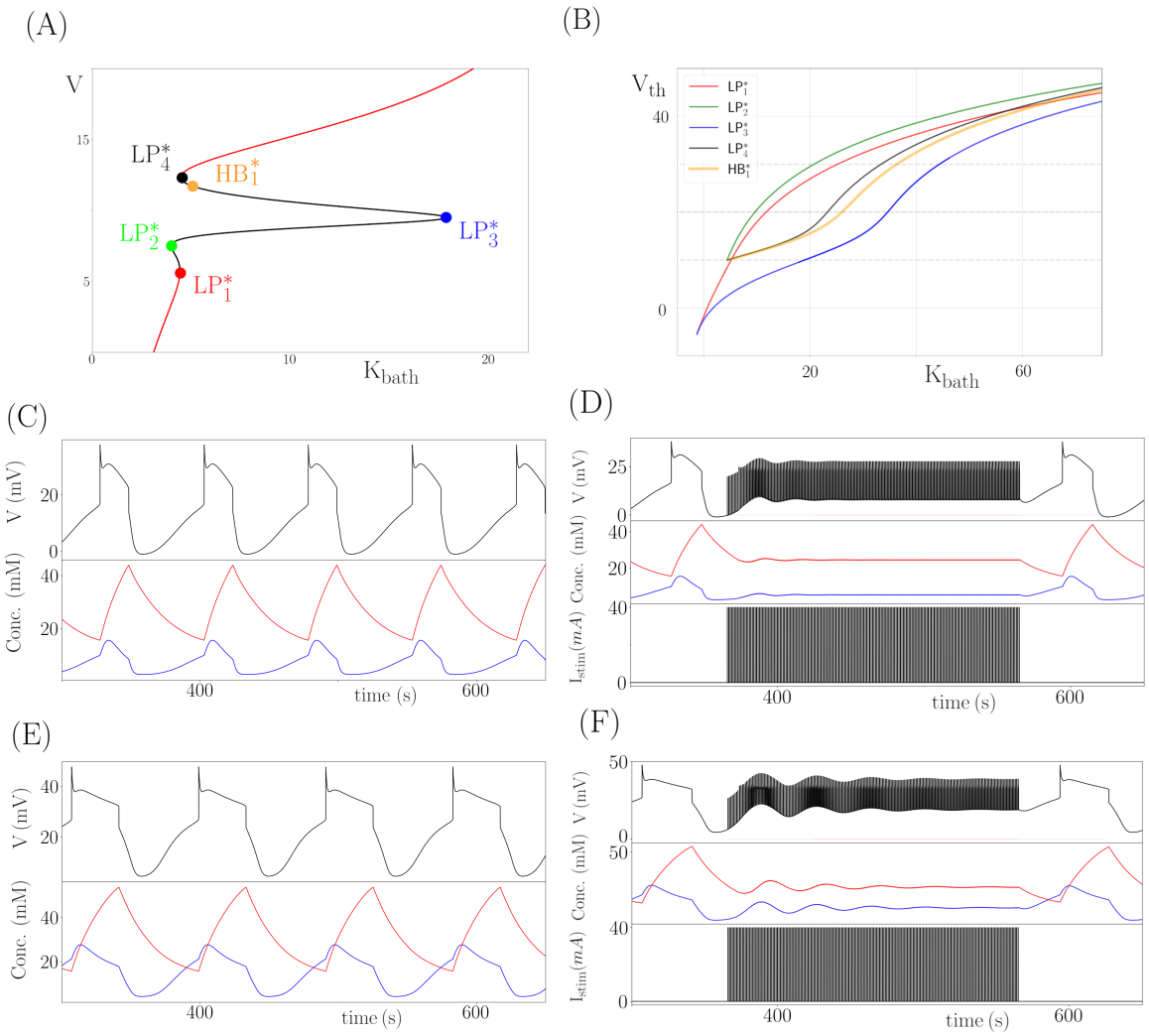

Figure S6: (A) Bifurcation diagram of V with respect to K_{bath} of the system Eq. Eq. (1), but with $g_{inh} = 0$. Black (resp. red) segments of the S-shaped curve of equilibria denote unstable (resp. stable) families of equilibria. (B) $\{K_{bath}, V_{th}\}$-parameter bifurcation diagram. HB* denotes Hopf bifurcation and LP*, fold bifurcation point. The three horizontal grey dashed lines are the different scenario we are studying in this figure : $V_{th} = 10, 20, 30$ mV. We also show the potential and ion dynamic time series for $V_{th} = 20$ mV and $K_{bath} = 15$mM ((C) unstimulated, (D) stimulated case); and for $V_{th} = 30$ mV and $K_{bath} = 29$mM ((E) unstimulated, (F) stimulated case). The potassium ion dynamic is the blue curve, and the sodium one is the red curve. The bifurcation diagram (A) shows that LP1 and LP4 are too close to allow clear seizure expression, prompting further analysis in the $\{K_{bath}, V_{th}\}$ space. By selecting $Vth = 20mV$ and $Vth = 30mV$, we demonstrate that seizure delay occurs without inhibition, justifying the inclusion of an inhibitory term to better reflect neuronal interactions.